Revista Brasileira de Geofísica
RBGf
Brazilian Journal of Geophysics

Revista Brasileira de Geofísica (2016) 34(4): 469-477

ISSN 0102-261X
www.scielo.br/rbg

OBSERVATIONS OF SMALL-SCALE GRAVITY WAVES IN THE EQUATORIAL UPPER MESOSPHERE

José André Vieira Campos[1], Igo Paulino[1], Cristiano Max Wrasse[2], Amauri Fragoso de Medeiros[1], Ana Roberta Paulino[1] and Ricardo Arlen Buriti[1]

ABSTRACT. Using airglow images collected at São João do Cariri (7.4°S; 36.5°W) from 2009 to 2010, the spectral characteristics and seasonality in the propagation direction of small-scale gravity waves were studied. There was a preferential propagation direction of the gravity waves to the east during the summer and spring. However, in the autumn and winter, the waves preferred propagate to the north. These observations can be related to the sources of the gravity waves or due to the filtering process of the wind on the vertical propagation of them. When gravity waves propagate in the same direction of the wind, they can reach critical levels and the vertical propagation of the waves are not allowed. Using wind profiles obtained from the Horizontal Wind Model – 14 (HWM-14), it was constructed blocking diagram in each level of the atmosphere to such areas where the vertical propagation of gravity waves was not permitted. These blocking regions change substantially along the seasons and can be used to explain the observed patterns in the propagation direction of the gravity waves.

Keywords: airglow, neutral wind, gravity waves, blocking diagram.

RESUMO. Utilizando imagens de aeroluminecência coletadas por um imageador instalado em São João do Cariri (7,4°S; 36,5°W) no período de 2009 a 2010, foram estudadas as características espectrais bem como a sazonalidade na direção de propagação de ondas de gravidade de pequena escala. Foi verificada uma preferência de propagação para leste no verão e na primavera, já no outono e inverno foi observada uma direção preferencial de propagação para norte. Estes resultados podem estar relacionados tanto às fontes que geram estas ondas de gravidade, quanto ao efeito de filtragem dos ventos sobre a região de estudo. As ondas de gravidade que se propagam no mesmo sentido do vento encontram níveis críticos e são filtradas. Com a utilização de perfis de vento obtidos pelo modelo "Horizontal Wind Model" – 14 (HWM-14) foi possível construir, em cada nível da atmosfera, as regiões de bloqueio para as quais a propagação vertical de ondas de gravidade não é permitida. Essas regiões de bloqueio sofreram mudanças sazonais substanciais e explicam satisfatoriamente os padrões observados na direção de propagação das ondas de gravidade.

Palavras-chave: aeroluminescência, vento neutro, ondas de gravidade, diagrama de bloqueio.

[1]Universidade Federal de Campina Grande, Av. Aprigio Veloso, 882, Bairro Universitário, 58429-140 Campina Grande, PB, Brazil. Phone/Fax: +55(83) 2101-1196 – E-mails: joseandrecampos@gmail.com; igopaulino@gmail.com; afragoso@df.ufcg.edu.br; arspaulino@gmail.com; rburiti@df.ufcg.edu.br

[2]Instituto Nacional de Pesquisas Espaciais, Avenida dos Astronautas, 1758, Jardim da Granja, 12227-010 São José dos Campos, SP, Brazil. Phone/Fax: +55(12) 3208-7740 – E-mail: cristiano.wrasse@inpe.br

INTRODUCTION

One of the most important properties of the atmosphere is the capability of supporting undulatory motions. These oscillation can be classified according to the temporal and spatial scales and/or the generating mechanisms. When a parcel of air is disturbed due to the pressure gradient and the gravitational force, the waves generated by this oscillation are named of gravity waves. The main role of the gravity waves in the atmosphere is transfer energy and momentum from the lower to the middle and upper atmosphere (Fritts & Alexander, 2003; Alexander et al., 2010; Fritts et al., 2012; Smith et al., 2015; Moss et al., 2016).

Several chemical processes can be found in the mesosphere and lower thermosphere (MLT), among them, there are airglow emissions, like OH, NaD, O_2, and OI557.7 nm (OI5577), which can be used as tracer to investigate gravity waves activities (Medeiros et al., 2005; Taylor et al., 2009, for instance). One of the most important technique to study gravity waves is the airglow imaging using all sky imagers, which produce two-dimensional images of the airglow for several emissions (e.g., Taylor et al., 1997; Taylor, 1997; Gardner et al., 1999; Medeiros et al., 2004; Li et al., 2011; Tang et al., 2014). By applying two-dimensional spectral analysis in the airglow images, it is possible to estimate the horizontal parameters of the gravity waves i.e., observed period and horizontal wavelength, phase speed and propagation direction (e.g., Wrasse et al., 2006; Taylor et al., 2009).

According to the spatial size (wavelength) and the shapes of the wave structures, the gravity waves can be classified as bands or ripples (Taylor et al., 1995). Band gravity waves appear frequently in the MLT and have tens of kilometers of wavelength, long extension in the airglow images and can persists over eight hours in the images during the night. On the other hand, ripples have small scales (short wavelength and periods) when seen in the airglow images and are transient wave events.

Gravity waves can also be classified by the horizontal wavelength as small scale (Medeiros et al., 2003; Wrasse et al., 2006) or medium-scale (Taylor et al., 2009; Takahashi et al., 2009; Paulino et al., 2011, 2016). Bands are typical examples of small scale gravity waves. There are other classifications to the gravity waves, e.g., traveling ionospheric disturbances (Narayanan et al., 2014) and mesospheric fronts (Fechine et al., 2005; Medeiros et al., 2016).

The present work describes the characteristics of 514 band gravity waves, observed from 2009 to 2010, in images of the OH airglow layer over São João do Cariri (7.4°S; 36.5°W). Furthermore, the seasonality in the propagation direction of the gravity waves were investigated considering the wind filtering process by using the background wind from the Horizontal Wind Model (HWM).

INSTRUMENTATION AND METHODOLOGY

All sky imager

Gravity waves were observed from 2009 to 2010 using an all sky imager, which allows one to make high resolution images of the nightglow. The all sky imager is composed by an optical system, a filter wheel and a Charge-Couple Device (CCD). The instrument is able to detect the variations in the nightglow.

The optical system has a fish-eye lens with a 180° field of view, which is used to observe the whole sky. There is also a system of lenses to project the light perpendicular to the interference filters and another one to conduct the image onto the CCD camera.

A filter wheel is used to select the desire airglow emission to be observed. In this equipment, OH NIR, O_2 (0,1), OI 557.7 nm (OI5577), OI 630.0 nm (OI6300) and background (BG) filters were used. The light crosses the interference filters and the focus is over the CCD sensor where is converted to a digital signal, i.e., digital image and it is stored in the hard drive of a personal computer. More details of the São João do Cariri's imager have been published elsewhere (Medeiros et al., 2003).

In order to investigate the gravity waves images from the OH airglow emission were used. Those images had an integration time of $\sim$15 s and a temporal resolution of $\sim$2 min which allows to follow the evolution of small-scale gravity waves.

Image Analysis

In order to calculate the gravity waves parameters, two dimensional Fast Fourier Transform (FFT) was used in a set of consecutive images. Wrasse et al. (2007) describes in details the cross spectrum analysis used in the present work to calculate the gravity waves parameters like horizontal wavelength, observed period and observed phase speed and the propagation direction.

Figure 1 shows some of the steps used to calculate the gravity wave parameters. Figure 1(A) shows a raw image collected at São João do Cariri on 23 September 2009. Figure 1(B) shows the unwarped and removed stars image. Figure 1(C) shows the results of the cross spectrum applied in the selected region shown and zoomed in 1(B) for a sequence of images. The red circles represents the amplitude of the gravity wave and the position of the amplitude also gives the information of the horizontal wavelength and the propagation direction (to North).

The observed gravity wave parameters described in Figure 1 are shown in Table 1, i.e., the horizontal wavelength (λ_H),

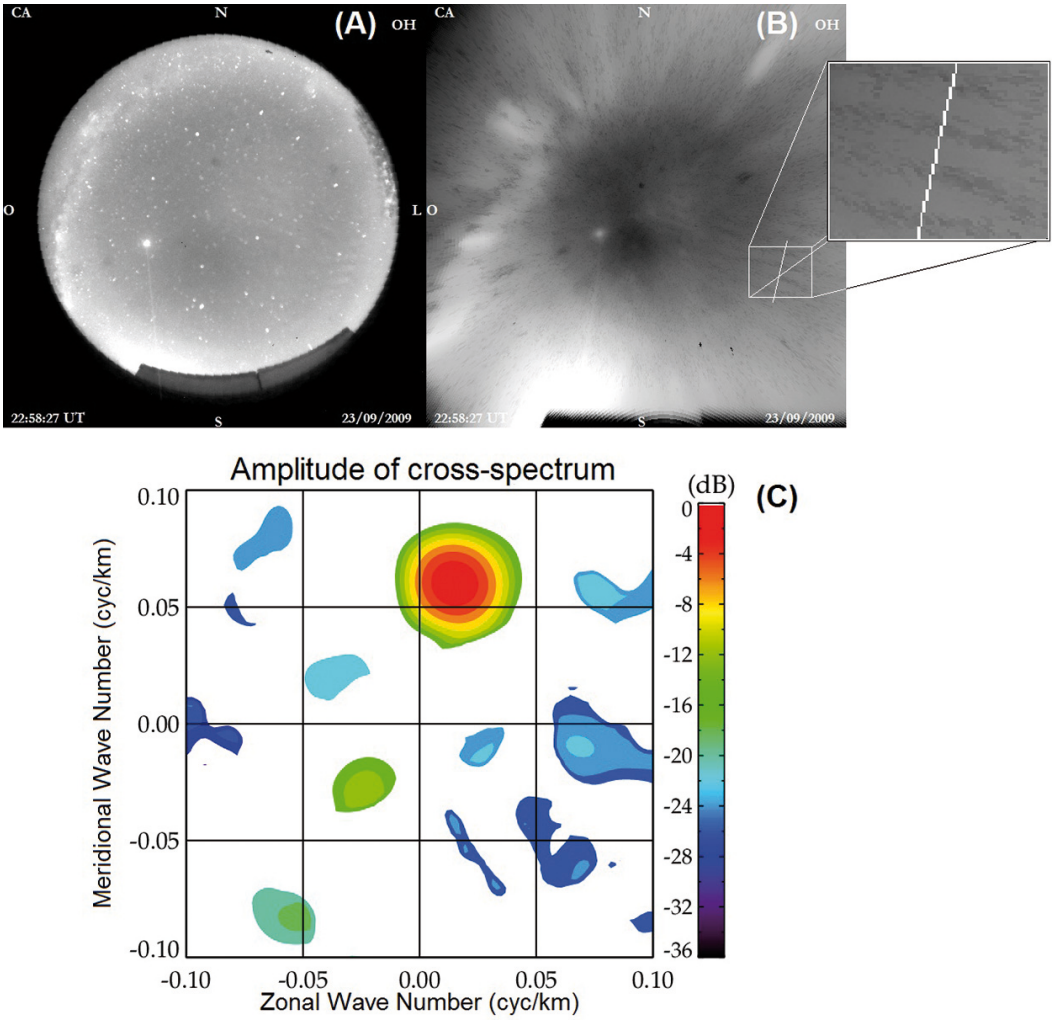

Figure 1 – (A) Raw image of the OH airglow emission observed at São João do Cariri on 23 September 2009. (B) Unwarped and remove stars image. A gravity wave event can be seen inside the box area, which was zoomed. (C) The amplitude of the cross spectrum applied to the select box in (B).

propagation direction (φ), phase speed (c), period (τ), zonal wavenumber (k) and meridional wavenumber (l). Typical error for these parameters were $< 10\%$ for the wavelength and $< 15\%$ for the period. Further details about the calculation of the parameters and errors can be found in Wrasse et al. (2007).

Wind filtering – Blocking diagrams

When gravity waves propagate vertically, they can reach turning levels or critical layers, which depends on the intensity and direction of the background blowing wind (Vadas, 2007). Critical layers or absorption levels appear ever the phase speed of the gravity waves approaches the background wind velocity. If the background wind is known throughout the atmosphere and assuming that the horizontal phase speed does not change when the wave propagates upward, it is possible to draw the regions where the phase speed of the gravity wave reaches a critical level. At these levels gravity waves are filtered and absorbed by the wind. The superposition of these regions are called blocking diagram (Medeiros et al., 2003).

The intrinsic frequency of the gravity wave, $\hat{\omega}$, under the influence of the horizontal wind can be described by Gossard & Hooke (1975, p. 122):

$$\hat{\omega} = \vec{k} \cdot (\vec{c} - \vec{v}), \tag{1}$$

were $\vec{k}$ is the horizontal wave vector, $\vec{c}$ is the wave phase speed and $\vec{v}$ is the horizontal wind as a function of altitude. When the waves move faster than the wind, $\hat{\omega}$ is positive, when move slower is negative. Defining $\vec{c} = \frac{\omega}{k}$, were ω is the angular or observed

Table 1 – Parameters of the gravity wave shown in Figure 1.

Date	λ_H km	φ (°)	c (m/s)	τ (min)	k (cyc/km)	l (cyc/km)
23/Sep/2009	16.2	18.4	21.0	12.8	0.01953	0.05859

frequency, the follow relation can be written:

$$\hat{\omega} = \omega \left(1 - \frac{\vec{v}}{\vec{c}}\right). \tag{2}$$

Equation 2 can also be rewritten as function of the zonal and meridional winds (v_z, v_m) as:

$$\hat{\omega} = \omega \left(1 - \frac{v_z \cos(\phi)\boldsymbol{i} + v_m \sin(\phi)\boldsymbol{j}}{\vec{c}}\right), \tag{3}$$

where $\boldsymbol{i}$ and $\boldsymbol{j}$ are unit vectores in the zonal (west-east) and meridional (sounth-north)directions, respectively. Thus, when a gravity waves reaches a critical layer, the background wind is equal to the wave phase speed ($\vec{v} = \vec{c}$), then $\hat{\omega} \rightarrow 0$ and the wave is absorbed. Using this condition, the following relation can be written:

$$\vec{c} = v_z \cos(\phi)\boldsymbol{i} + v_m \sin(\phi)\boldsymbol{j} \tag{4}$$

Equation 4 is used to represent the blocking diagram in a polar chart running the azimuthal angles from 0 to 360°. The winds, used as input were obtained from the Horizontal Wind Model – 2014 (HWM-14) (Drob et al., 2015). The numerical model gives the global horizontal wind from the surface up to hundreds of kilometers height. In this work, the blocking diagrams were calculated from the surface to 100 km for the São João do Cariri's geographical coordinates during the gravity wave observations. In order to understand the wind effects filtering the gravity waves, it was used the maximum wind magnitude during the nighttime within the season period to obtain the blocking diagrams. Using more realistic data, primary from measurements or reanalysis methods, the accuracy of the blocking diagram would be improved. However, it is out of the scope of the present work because the main contribution in this article is the statistical analysis of the propagation of the observed gravity waves.

Figure 2 shows the three dimensional blocking diagram for the four seasons of 2009.

The blocking diagrams shown in Figure 2 can be used to find out regions where $\hat{\omega} \leq 0$ (wave phase speed $\leq$ wind velocity), which corresponds to the prohibited regions for the vertical propagation of the gravity waves. They can also be used to investigate the preferential propagation direction of the gravity waves which may be in opposite direction of the blocking area. For instance, during summer time, the wind blows predominantly to west can indicate that the waves propagating eastward are more favorable to overcome the critical levels. However, if a gravity wave has horizontal phase speed higher than the a given blocking region, it can scape of the critical levels anyway, that is, independent of the propagation direction.

RESULTS AND DISCUSSION

Over 500 gravity waves were observed from 2009 to 2010, the histogram for the observed period (A) and horizontal wavelength (B) are shown in Figure 3. The results pointed out that 212 events were observed in 2009 (blue) and 302 events were observed in 2010 (green). Most of the wave periods ranged from 7 to 21 min in both years and had an average of 14 min in 2009 and 13 min in 2010. Regarding to the horizontal wavelength, most of them were larger than 12 km and shorter than 42 km, with averages of 26 km in 2009 and 27 km in 2010.

These results show that the spectral characteristics of the gravity do no change substantially from one year to another one. Furthermore, comparing the present result to the Medeiros et al. (2004) results for the same station, there was no much differences as in the horizontal wavelength as in the observed period ranges.

Figure 4(A) shows a polar chart for the propagation direction and the magnitude of the observed phase speed of the gravity waves (arrows). Figure 4(B) shows the polar histogram for the propagation direction of the gravity waves.

Most of the gravity waves shown in Figure 4(A) propagates to the east with mean phase speed of 37 m/s (39 m/s) $\pm$15 m/s for 2009 (2010). In average, the absolute values of the phase speed are not changing along these two years as well. The present phase speed results agree very well with the results presented by Medeiros et al. (2004).

Figure 4(B) shows an interesting result, in 2009 there were more gravity waves propagating to the northeast. On the other hand, in 2010, more gravity waves were observed propagating southeastward. However, it is clear that there is an anisotropy in the propagation direction of the gravity waves from the interior of the continent to the ocean direction. Two factors can create this

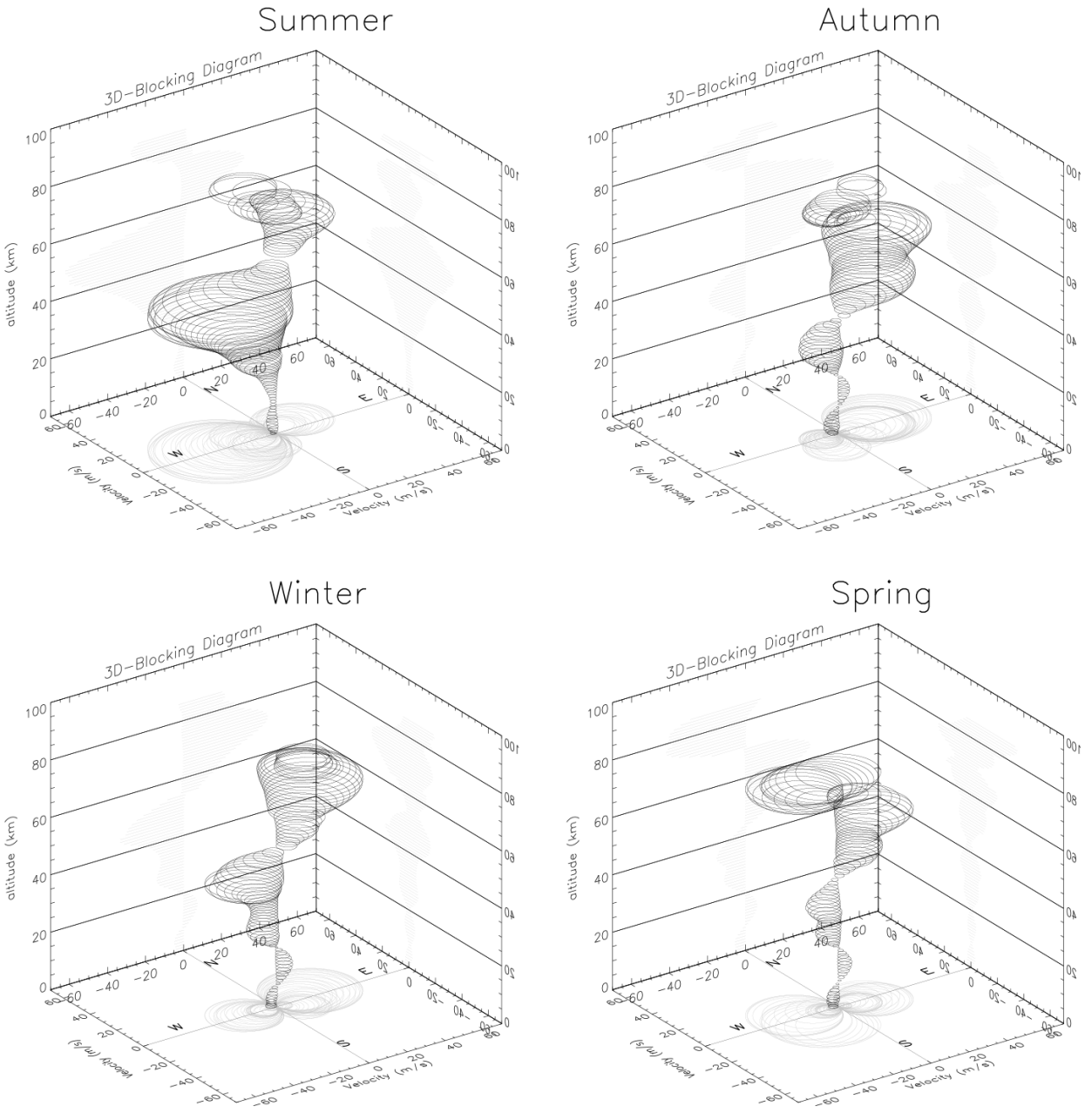

Figure 2 – Three dimensional blocking diagram, where the circles represent the critical layer region for gravity waves propagation. The circles are drawn at each 1 km.

anisotropy: (1) the location of the sources of the gravity waves and/or (2) the filtering process due to the background wind.

Wrasse et al. (2006) presented some results of the gravity wave sources for waves observed at São João do Cariri in 2001. The authors found that the wave sources are located in the west region of the observation site, with only 24% of them associated to tropospheric meteorological phenomena, and around 70% probably generated *in situ*.

In order to investigate the filtering process, the blocking diagrams are going to be used to explore more specifically the critical levels on the propagation of the gravity waves. The waves were separated according to the seasons.

Figure 5 shows the combining effect of the blocking diagrams projected in two-dimension with the phase speed of the gravity waves observed in 2009.

Figure 6 shows the two-dimensional blocking diagrams for

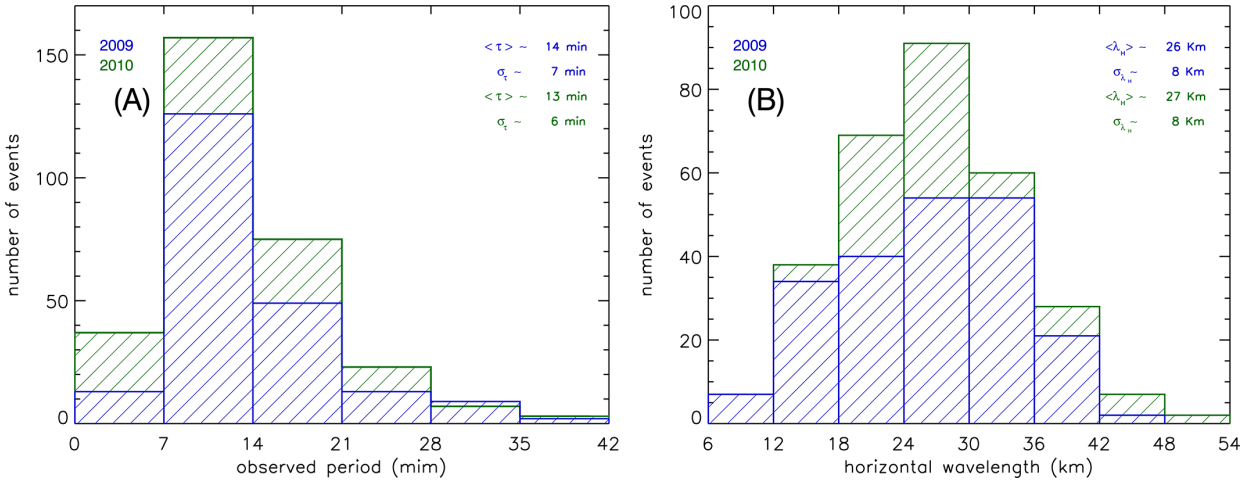

Figure 3 – Histograms for (A) observed period and for (B) horizontal wavelength. Blue bars represent the gravity waves observed in 2009 and green ones in 2010. The average and standard deviation are shown on the right top of the charts.

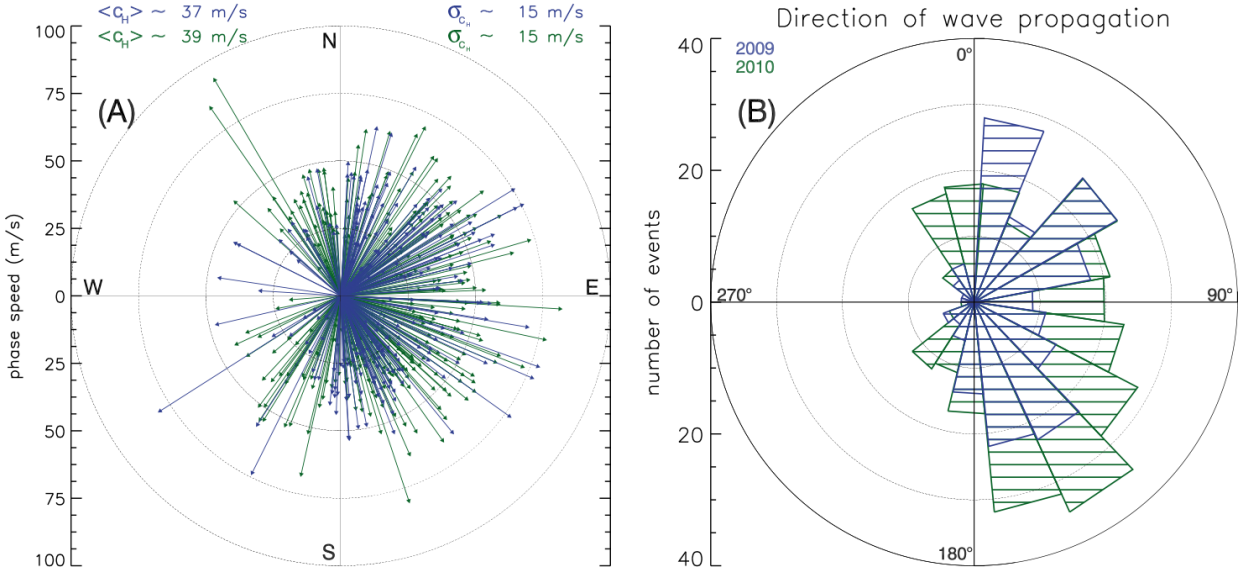

Figure 4 – (A) Polar chart for the phase speed vector of all observed gravity waves. (B) Polar histogram for the propagation direction of the gravity waves. The color patterns are the same shown in Figure 3.

the gravity waves observed during 2010.

One can note that the blocking diagrams appear ever in the opposite direction of the gravity waves propagation or they are smaller than the phase speed of most of the gravity waves. Figure 5 shows that, in the summer, the blocking area occur at the west side of the observatory and most of the gravity waves were propagating to the east, northeast or southeast, for instance. Further, most of the of the gravity waves, represented by the arrows, were outside of the blocking areas. Only a few of them reached the prohibited regions and it may be due to the average model winds that are being used to represent the seasonal wind system.

Comparing Figure 5 to Figure 6, it is possible to see a similar behavior in both studied years. The main difference was observed in the winter, where there were more gravity waves propagating to the south in 2010. These results suggest that the filtering process of the wind remains almost the same from a year to another.

The blocking diagrams explain very well the seasonal variability of the propagation direction of the gravity waves, i.e., they

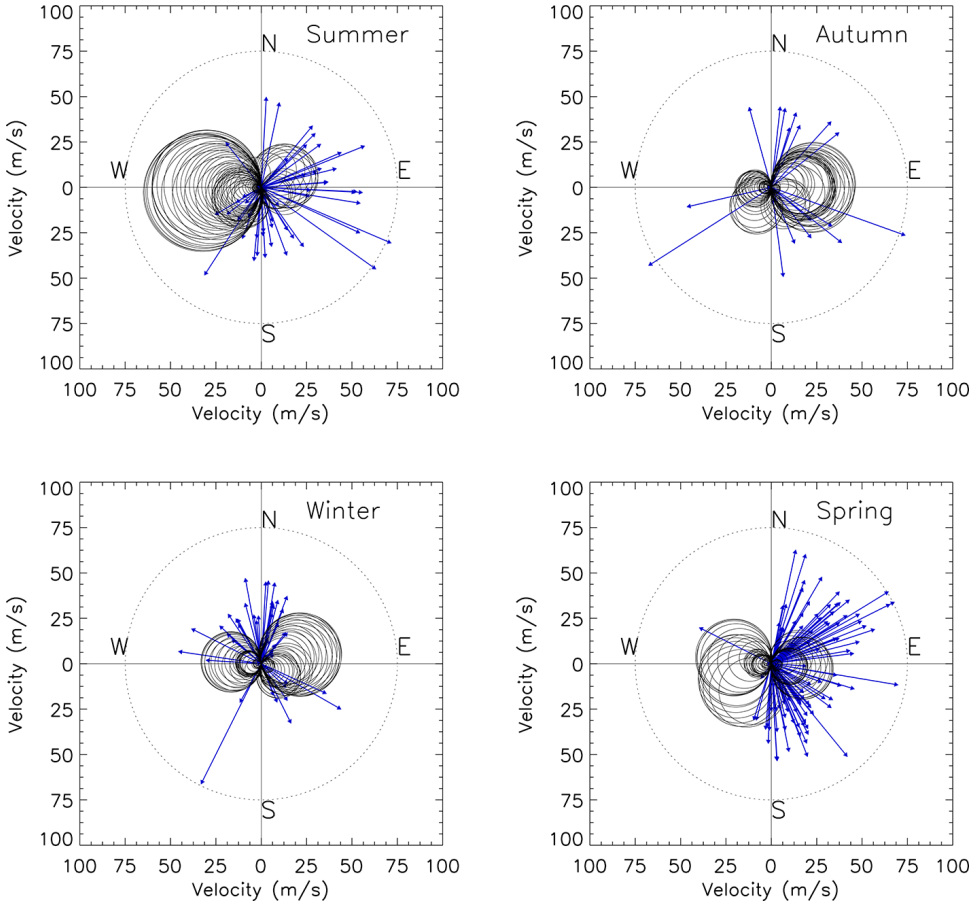

Figure 5 – Two dimensional projection of the blocking diagrams from Figure 2 combining the phase speed of the gravity waves observed in 2009.

suggest that the filtering of the gravity due to the wind may be the main mechanism to the observed the anisotropy and seasonality of the gravity waves. Of course, the location of the sources the gravity must be considered as well and it is very important to observed the present characteristics. Although if the sources were isotropically located around the São João do Cariri, even then, these anisotropies in the propagation direction of the gravity wave could be explained only by considering the filtering process.

The anisotropy of propagation direction of the gravity were also discussed by Medeiros et al. (2003) for the Cachoeira Paulista. They found different patterns for that because the characteristics of the gravity waves observed in Cachoeira Paulista were different from those observe in São João, but, they could explain the results using blocking diagram as well.

SUMMARY

Small-scale gravity waves were observed over São João do Cariri during 2009 and 2010, using an all sky imager. The spectral characteristics of the waves, i.e., horizontal wavelength, observed period and phase speed did not change significantly along of the two years of observation and they agree with previous observations for the same site.

A clear anisotropy in the gravity waves propagation direction were observed. Almost all waves were propagating to the east side of the observation site. There was also observed a seasonality in the propagation direction of the gravity waves. These two characteristics were well explained investigating the filtering process of the gravity wave propagation due to the background wind structure. Thus, the observation of small scale gravity waves in the MLT region must be strongly controlled by the wind system in the lower and primarily in the middle atmosphere.

ACKNOWLEDGEMENTS

J.A.V. Campos thanks the support of the Scientific Initiation Scholarship Program (PIBIC/UFCG-CNPq) under Process No. 164475/2014-1. I. Paulino and C.M. Wrasse thank to

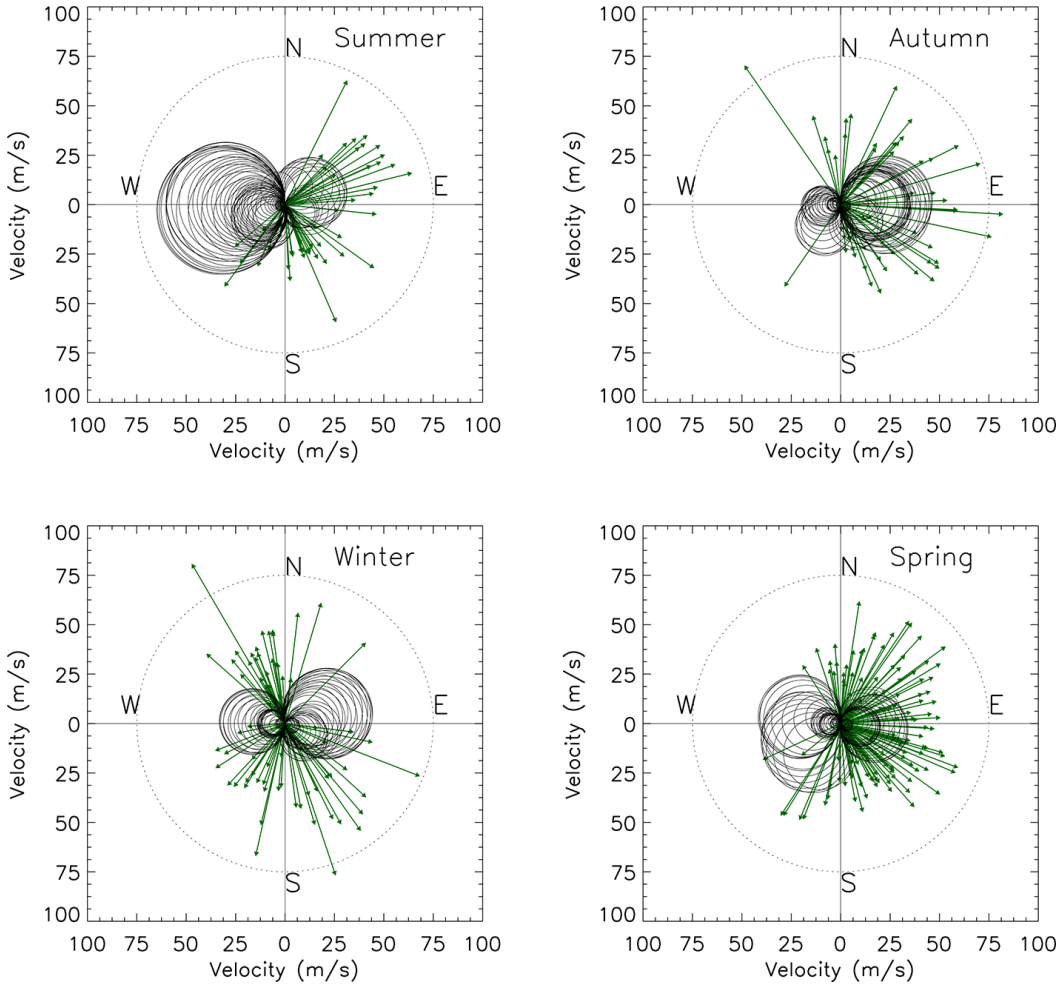

Figure 6 – Same as Figure 5, but for 2010.

Conselho Nacional de Desenvolvimento Científico e Tecnológico (CNPq) by the financial support under contracts 478117/2013-2 and 310926/2014-9, respectively.

REFERENCES

ALEXANDER M, GELLER M, McLANDRESS C, POLAVARAPU S, PREUSSE P, SASSI F, SATO K, ECKERMANN S, ERN M, HERTZOG A, KAWATANI Y, PULIDO M, SHAW T, SIGMOND M & VINCENT R. 2010. Recent developments in gravity-wave effects in climate models and the global distribution of gravity-wave momentum flux from observations and models. Quarterly Journal of the Royal Meteorological Society, 136: 1103–1124.

DROB DP, EMMERT JT, MERIWETHER JW, MAKELA JJ, DOORNBOS E, CONDE M, HERNANDEZ G, NOTO J, ZAWDIE KA, McDONALD SE, HUBA JD & KLENZING JH. 2015. An update to the Horizontal Wind Model (HWM): The quiet time thermosphere. Earth and Space Science, 2: 301–319, doi: 10.1002/2014EA000089, URL <http://dx.doi.org/10.1002/2014EA000089>.

FECHINE J, MEDEIROS A, BURITI R, TAKAHASHI H & GOBBI D. 2005. Mesospheric bore events in the equatorial middle atmosphere. Journal of Atmospheric and Solar-Terrestrial Physics, 67: 1774–1778.

FRITTS DC & ALEXANDER MJ. 2003. Gravity wave dynamics and effects in the middle atmosphere. Reviews of Geophysics, 41(1): 1003.

FRITTS D, JANCHES D, HOCKING W, MITCHELL N & TAYLOR MJ. 2012. Assessment of gravity wave momentum flux measurement capabilities by meteor radars having different transmitter power and antenna configurations. Journal of Geophysical Research: Atmospheres, 117.

GARDNER CS, GULATI K, ZHAO Y & SWENSON G. 1999. Measuring gravity wave momentum fluxes with airglow imagers. Journal of Geophysical Research: Atmospheres, 104: 11 903–11 915, doi: 10.1029/1999JD900105, URL <http://dx.doi.org/10.1029/1999JD900105>.

LI Z, LIU AZ, LU X, SWENSON GR & FRANKE SJ. 2011. Gravity wave characteristics from OH airglow imager over Maui. Journal of Geophysical Research: Atmospheres, 116.

MEDEIROS A, TAYLOR MJ, TAKAHASHI H, BATISTA P & GOBBI D. 2003. An investigation of gravity wave activity in the low-latitude upper mesosphere: Propagation direction and wind filtering. Journal of Geophysical Research: Atmospheres (1984-2012), 108.

MEDEIROS AFD, BURITI R, MACHADO E, TAKAHASHI H, BATISTA PP, GOBBI D & TAYLOR MJ. 2004. Comparison of gravity wave activity observed by airglow imaging at two different latitudes in Brazil. Journal of Atmospheric and Solar-Terrestrial Physics, 66: 647–654.

MEDEIROS A, FECHINE J, BURITI R, TAKAHASHI H, WRASSE C & GOBBI D. 2005. Response of OH, O_2 and OI5577 airglow emissions to the mesospheric bore in the equatorial region of Brazil. Advances in Space Research, 35: 1971–1975.

MEDEIROS A, PAULINO I, TAYLOR M, FECHINE J, TAKAHASHI H, BURITI R, LIMA L & WRASSE C. 2016. Twin mesospheric bores observed over Brazilian equatorial region. Annales Geophysicae, 34: 91–96.

MOSS A, WRIGHT C, DAVIS R & MITCHELL N. 2016. Gravity-wave momentum fluxes in the mesosphere over Ascension Island (8°S, 14°W) and the anomalous zonal winds of the semi-annual oscillation in 2002. Annales Geophysicae, 34: 323–330.

NARAYANAN VL, SHIOKAWA K, OTSUKA Y & SAITO S. 2014. Airglow observations of nighttime medium-scale traveling ionospheric disturbances from Yonaguni: Statistical characteristics and low-latitude limit. Journal of Geophysical Research: Space Physics, 119: 9268–9282, doi: 10.1002/2014JA020368, URL <http://dx.doi.org/10.1002/2014JA020368, 2014JA020368>.

PAULINO I, TAKAHASHI H, MEDEIROS A, WRASSE C, BURITI R, SOBRAL J & GOBBI D. 2011. Mesospheric gravity waves and ionospheric plasma bubbles observed during the COPEX campaign. Journal of Atmospheric and Solar-Terrestrial Physics, 73: 1575–1580, doi: http://dx.doi.org/10.1016/j.jastp.2010.12.004.

PAULINO I, MEDEIROS A, VADAS S, WRASSE C, TAKAHASHI H, BURITI R, LEITE D, FILGUEIRA S, BAGESTON J, SOBRAL J & GOBBI D. 2016. Periodic waves in the lower thermosphere observed by OI630 nm airglow images. Annales Geophysicae, 34: 293–301.

SMITH SM, MARTINIS CR, BAUMGARDNER J & MENDILLO M. 2015. Allsky imaging of transglobal thermospheric gravity waves generated by the March 2011 Tohoku Earthquake. Journal of Geophysical Research: Space Physics, 120.

TAKAHASHI H, TAYLOR MJ, PAUTET P-D, MEDEIROS AF, GOBBI D, WRASSE CM, FECHINE J, ABDU MA, BATISTA IS, PAULA E, SOBRAL JHA, ARRUDA D, VADAS SL, SABBAS FS & FRITTS DC. 2009. Simultaneous observation of ionospheric plasma bubbles and mesospheric gravity waves during the SpreadFEx Campaign. Annales Geophysicae, 27: 1477–1487, doi: 10.5194/angeo-27-1477-2009, URL <http://www.ann-geophys.net/27/1477/2009/>.

TANG Y, DOU X, LI T, NAKAMURA T, XUE X, HUANG C, MANSON A, MEEK C, THORSEN D & AVERY S. 2014. Gravity wave characteristics in the mesopause region revealed from OH airglow imager observations over Northern Colorado. Journal of Geophysical Research: Space Physics, 119: 630–645.

TAYLOR MJ. 1997. A review of advances in imaging techniques for measuring short period gravity waves in the mesosphere and lower thermosphere. Advances in Space Research, 19: 667–676.

TAYLOR MJ, GU Y, TAO X, GARDNER C & BISHOP M. 1995. An investigation of intrinsic gravity wave signatures using coordinated lidar and nightglow image measurements. Geophysical Research Letters, 22: 2853–2856.

TAYLOR MJ, PENDLETON W, CLARK S, TAKAHASHI H, GOBBI D & GOLDBERG R. 1997. Image measurements of short-period gravity waves at equatorial latitudes. Journal of Geophysical Research: Atmospheres, 102: 26 283–26 299.

TAYLOR MJ, PAUTET P-D, MEDEIROS A, BURITI R, FECHINE J, FRITTS D, VADAS S, TAKAHASHI H & SÃO SABBAS F. 2009. Characteristics of mesospheric gravity waves near the magnetic equator, Brazil, during the SpreadFEx campaign. Annales Geophysicae, 27: 461–472.

VADAS SL. 2007. Horizontal and vertical propagation and dissipation of gravity waves in the thermosphere from lower atmospheric and thermospheric sources. Journal of Geophysical Research: Space Physics, 112.

WRASSE C, NAKAMURA T, TAKAHASHI H, MEDEIROS A, TAYLOR MJ, GOBBI D, DENARDINI C, FECHINE J, BURITI R, SALATUN A, SURATNO, ACHMAD E & ADMIRANTO AG. 2006. Mesospheric gravity waves observed near equatorial and low-middle latitude stations: wave characteristics and reverse ray tracing results. Annales Geophysicae, 24: 3229–3240.

WRASSE CM, TAKAHASHI H, MEDEIROS AFD, LIMA LM, TAYLOR MJ, GOBBI D & FECHINE J. 2007. Determinação dos parâmetros de ondas de gravidade através da análise espectral de imagens de aeroluminescência. Brazilian Journal of Geophysics, 25(3): 257–266.

Recebido em 28 outubro, 2016 / Aceito em 15 maio, 2017
Received on October 28, 2016 / Accepted on May 15, 2017